ELSEVIER

International Journal of Mass Spectrometry 179/180 (1998) 27–42

International Journal of Mass Spectrometry

Theoretical analysis of ethylene adducts to ion-bombarded porous silica

Nazzareno Re[a], Antonio Sgamellotti[a,*], Gianfranco Cerofolini[b]

[a]*Dipartimento di Chimica e Centro di Studio CNR per il Calcolo Intensivo in Scienze Molecolari, Università di Perugia, via Elce di Sotto 8, 06123 Perugia, Italy*
[b]*SGS-Thomson Microelectronics, 20041 Agrate, Italy*

Received 16 February 1998; accepted 22 July 1998

Abstract

Density functional calculations have been performed on molecular models of silica defects and their C_2H_4 adducts. The results are consistent with a previous experimental infrared characterization that was interpreted in terms of C_2H_4 addition to the SiO_2 skeleton at both the oxygen-bridge and silicon-link vacancy defects produced by argon bombardment. The geometries and thermodynamical stabilities of the proposed species and other possible adducts have been evaluated. The calculated C═C, C═O and C–H stretching frequencies are in good agreement with the experimental values and confirm the validity of the previous interpretation, helping to clarify some unclear details. (Int J Mass Spectrom 179/180 (1998) 27–42) © 1998 Elsevier Science B.V.

Keywords: Solid matrix functionalization; Gas-solid reactions; Ion bombardment; Density functional calculations; Porous silica

1. Introduction

Ion bombardment (IB) in a controlled atmosphere is a new method for functionalizing disperse targets. The test vehicle for this technique was the bombardment of porous SiO_2 in a CO_2 [1] or C_2H_4 [2] atmosphere. The grounds of this technique are described in the following. The native defects that are expected to be produced during IB are the oxygen-bridge vacancy (OBV),

≡Si· ·Si≡ (**A**)

(usually referred to as E″ centre) and the silicon-link vacancy (SLV),

≡Si–O· ·O–Si≡ (**B**)

≡Si–O· ·O–Si≡

According to the allowed relaxation processes, the OBV may assume one or the other of the following configurations: (1) The SiO_2 relaxes, reducing the Si–Si distance in such a way that a Si–Si bond can actually be formed:

≡Si· ·Si≡ → ≡Si–Si≡ (**C**)

The energetics of this process were already studied by the present authors, who showed that the bond energy depends strongly on strain. (2) The SiO_2 relaxes, increasing the Si–Si distance, and in this way allows

* Corresponding author.

Dedicated to Professor Fulvio Cacace in recognition of his outstanding contributions for many decades to gas-phase ion chemistry and physics.

PII S1387-3806(98)14128-3

the silicon radicals not to perturb each other. The centre has no way to relax and survives as a diradical (usually known as E″ centre) until it reacts with ambient molecules. (3) The ionic electronic state $\equiv Si^{+}\ ^{-}Si\equiv$ of the E″ centre has an excitation energy of about 8 eV [3], so that it cannot be obtained by thermal excitation. This state, however, can be stabilized by the formation of a Lewis adduct between the positively charged silicon and a siloxane or silanol oxygen:

$$\equiv Si^{+} + :O\langle \rightarrow \equiv Si^{+} \leftarrow :O\langle \qquad (1)$$

with a stabilization energy of ~5 eV [3]. It is not surprising, therefore, that in condensed matter the configuration [$\equiv Si^{+} \leftarrow :O\langle\ ^{-}Si\equiv$] (**D**) may have, according to the actual relaxation process, formation enthalpies comparable with that of $\equiv Si–Si\equiv$. This ionic state, first hypothesized by Rudra and Fowler [4], has been demonstrated to be a metastable configuration for α quartz with a "puckered" geometry and a silicon–silicon distance of ~4 Å [5–7].

In the study of the reactivity of the ion-bombarded SiO_2, one has to consider all these states, although $\equiv Si–Si\equiv$ is expected to manifest a modest reactivity.

The SLV is expected to relax either to a partial peroxidated silicon vacancy (PSV),

$$\equiv Si–O–O–Si\equiv \qquad (\mathbf{E})$$

$$\equiv Si–O^{\cdot}\ \ ^{\cdot}O–Si\equiv$$

or to a total PSV,

$$\equiv Si–O–O–Si\equiv \qquad (\mathbf{F})$$

$$\equiv Si–O–O–Si\equiv$$

Because of the presence of radical pairs in the native defects **A** and **B** and in the partially relaxed one, **E**, these defects are expected to be strongly reactive, and able to add foreign molecules with still unexplored pathways. The reactivity of the relaxed defects **C** and **F** is associated with the ability of the foreign molecule to cleave efficiently the Si–Si bond and the peroxidic bridge, respectively. Strain effects make this task easier. The radical defects are expected to react even with the residual gases of the atmosphere over the target during the bombardment, so that *the unique way to have a controlled addition to the SiO_2 skeleton is to carry out the IBB in a controlled atmosphere*; this reason motivated this technique of silica doping.

In the first set of experiments, where the IB was carried out in a CO_2 atmosphere, this molecule was efficiently added to the SiO_2 skeleton via the formation of a carboxylate group [9], a group that is hardly grafted to silica with any other synthetic pathway. This conclusion, based on infrared spectroscopic data, was confirmed by both ab initio molecular dynamics simulations of the interactions of CO_2 with the E″ centre [1] and accurate density functional calculations [9].

Having the experiments of [1] (based on the reactivity toward CO_2) clarified the presence and reactivity of the E″ centre, Cerofolini et al. decided to study the presence and the reactivity of the other expected native defect: the SLV and its relaxed configurations. For that, the IBB was performed in a C_2H_4 atmosphere. Ethylene was chosen because its reaction with the E″ and SLV centres seemed predictable [2], as confirmed by the experimental evidence that is briefly described in the next paragraph.

To support the interpretation of the above IB experiments, in this article we have performed ab initio density functional theory (DFT) calculations on suitable molecular models of the OBV and SLV silica defects and their C_2H_4 adducts to give a quantitative account of the experimental data of [2].

2. Survey of experimental investigations

The addition of C_2H_4 into ion-bombarded porous SiO_2 was studied by implanting $^{40}Ar^{2+}$ at an acceleration voltage of 150 kV and at a fluence of 5×10^{14} cm^{-2} onto a porous silica target kept under a C_2H_4 atmosphere [2]. The bombarded sample was subsequently aged at room temperature in a nitrogen atmosphere or in air and then annealed at 500 °C in a vacuum. Fourier transform infrared (IR) absorption measurement and x-ray photoelectron spectroscopy (XPS) analysis were carried out on: (1) the bombarded sample after aging of 100 h in a nitrogen atmosphere; (2) bombarded sample after aging of

100 h in a nitrogen atmosphere and then heated in vacuum at 500 °C for 0.5 h; (3) bombarded sample kept a few hours in a nitrogen atmosphere; and (4) bombarded sample kept a few hours in a nitrogen atmosphere exposed for 72 h to air at room temperature. The IR spectra of as-implanted samples exhibit peaks located at 2970 cm^{-1}, 2936 cm^{-1}, 2880 cm^{-1}, 2860 cm^{-1}, and 1710 cm^{-1}, 1603 cm^{-1}, and 1583 cm^{-1}, together with OH stretchings that are not related to ethylene addition. The peaks at 2970 cm^{-1} and 2880 cm^{-1} were attributed to the antisymmetrical and symmetrical vibrations, respectively, of the CH_3 group. Similarly, the peaks at 2936 cm^{-1} and 2860 cm^{-1} were attributed to the antisymmetrical and symmetrical vibrations, respectively, of the CH_2 group. These peaks are, however, shifted by 5–10 cm^{-1} toward higher frequencies with respect to the values characteristic of alkanes. The peak at 1710 cm^{-1} was attributed to the C═O group: its value is characteristic of the C═O stretching in liquid acetic aldehyde CH_3CHO. The peaks at 1583 cm^{-1} and 1603 cm^{-1} are in the range of C═C bond stretching; they were attributed to ethylene, although the shift from the value for the free molecule and the presence of a satellite peak at 1640 cm^{-1} suggest that ethylene is not simply physisorbed, but rather forms coordination adducts. The absence of distorted OH peaks shows that ethylene is not adsorbed on silanols. Annealing at 500 °C led to the almost complete disappearence of the C═C and C═O signals, a reduction of the CH_3 peaks by a factor of 2, and a strengthening of the CH_2 peaks. Moreover, the frequencies of the CH_2 peaks are shifted with respect to the proper values of alkanes.

Fig. 1 sketches some plausible adducts of C_2H_4 to the E″ centre proposed in [2]. Adduct **1** is expected to occur via an acid-base pathway, whereas **2**, **3**, and **4** would be formed via radical pathway. Fig. 2 shows a plausible radical pathway adding C_2H_4 to an SLV or partial PSV. The reaction would involve first the cleavage of the π bond of C_2H_4 by a siloxyl in **5** and the formation of a carbon radical in **6**, then hydrogen abstraction by another siloxyl (attack by a free radical at a univalent atom of a substrate molecule is indeed known to occur in radical reaction [2]) and the

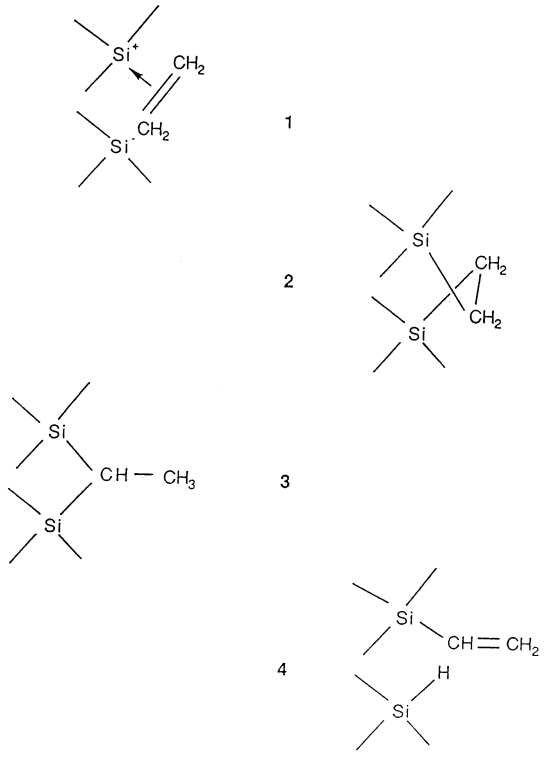

Fig. 1. Expected adducts formed by the OBV defect with C_2H_4.

formation of two close carbon radicals in **7** that eventually recombine via the formation of a π bond. This pathway leads to the formation of a centre, **8**, in which the organic part is grafted to silica through an oxygen bridge.

Actually, a distorted C═C signal was detected, thus making plausible the attribution to C_2H_4 in a coordinated configuration like **1**. Similarly, two peaks that can be attributed to a CH_2 vibration were observed; the frequency peak value, at 2936 cm^{-1} in the as-implanted sample versus 2930 cm^{-1} in alkanes, could be explained by assuming that ethylene addition at room temperature to the E″ centre occurs via a strained configuration without complete stress relaxation. This conclusion is consistent with the fact that $-CH_2–CH_2-$ bridging between silicon radicals cannot occur without straining (see **2** in Fig. 1). The presence of the CH_3 signal even after high-temperature annealing suggested its stable insertion in adducts like **3**, whereas the absence of any Si–H signal

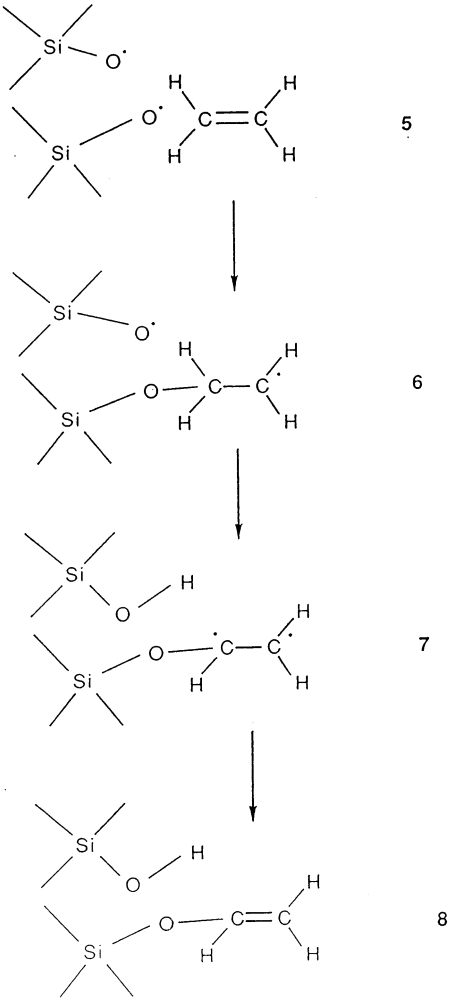

Fig. 2. Mechanism suggested for the formation of a C_2H_4 adduct on a SLV.

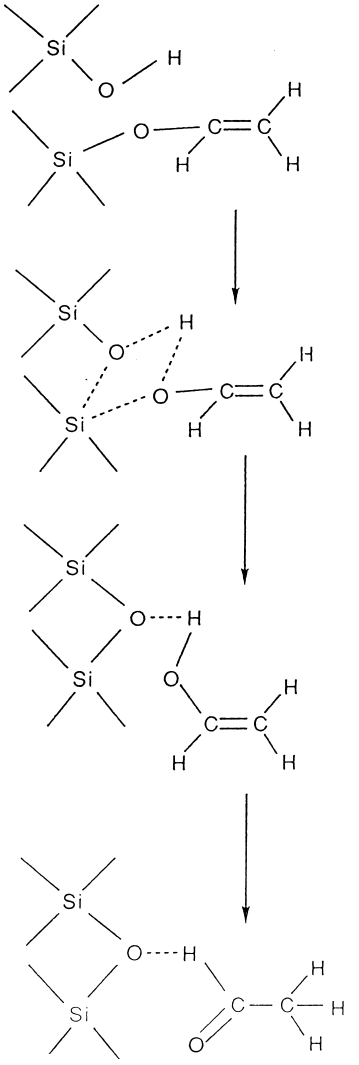

Fig. 3. Reaction leading to acetyc aldehyde.

suggests that the pathway leading to the centre **4** is highly improbable.

Much more problematic was understanding the reaction of C_2H_4 with the SLV. The observation that the CH_3 and C═O peaks evolve synchronously, irrespective of the fact that—according to the process undergone—they either increase or decrease (see [2]), suggested that they are formed in pairs as reaction products of C_2H_4 plus SLV. The evolution of centre **8** to acetic aldehyde and a silanol group (Fig. 3) was hypothesized. In proposing the above interpretation, Cerofolini et al. were well aware of its rather speculative character. As discussed in [2], the uncertainty in the interpretation cannot be removed resting on the experimental side alone because of the unavailability of model molecules that mimic the adducts formed by the reaction of bombarded silica with ethylene. To overcome this difficulty, and encouraged by the strong support of the interpretation of the SiO_2–CO_2 system provided by quantum theoretical analysis, we have decided to extend the procedure to the SiO_2–C_2H_4 system.

3. Models and theoretical methods

To model the OBV defect, we have used two $(OH)_3Si^{\cdot}$ molecular radicals for the diradical configuration **A** or two ions, $(OH)_3Si^+$ and $(OH)_3Si^-$, for the ionic configuration **D**, whereas for the SLV defect we have used two $(OH)_3Si–O^{\cdot}$ radicals. All the proposed C_2H_4 adducts were modeled by the corresponding molecular compounds in which the silica centres have been substituted by $(OH)_3Si-$ groups (see below). Such an approach in which small discrete molecules are employed to simulate the behaviour of solid substructures has been applied to several systems [10]. Although it neglects any interaction within the three-dimensional framework, this approach has been successfully employed to simulate the behaviour of silica, silicate functional groups, zeolites and surface silica hydroxyls [7, 10–13]. Some of the C_2H_4 adducts on the OBV defects proposed in this work involve a bridge between two silicon atoms and have been modeled by molecules with two silicon atoms like $(HO)_3Si–CH_2–CH_2–Si(OH)_3$. Unfortunately, such a molecular model allows a complete relaxation of the two $Si(OH)_3$ groups at variance with the actual situation in the solid silica where a full relaxation is hampered by the rigid structure of the three-dimensional network. This effect has been simulated by employing more realistic models of the actual silica structure, based on a cyclic molecule with two or three silicon atoms connected by siloxanic bridges (see below).

Reaction energies have been evaluated using the optimized energies of the considered molecular models of the ethylene adducts to OBV and SLV defects. However, in order to account for the constraints of the silica network on the geometry of the OBV defect, we used the energy of the unoptimized $(OH)_3Si^{\cdot}$ and $(OH)_3Si^+$ species, taking a pyramidal geometry from the optimized $(OH)_3Si–O–Si(OH)_3$ molecule. This choice only slightly affects (less than 10 kJ mol^{-1}) the reaction energies for C_2H_4 addition to the diradical centre, but has significant consequences on the reaction energies for C_2H_4 addition to the ionic configuration. Indeed, the $(OH)_3Si^+$ shows a high relaxation energy (more than 200 kJ mol^{-1}) from the pyramidal to the essentially planar optimized geometry. We expect that the rigid three-dimensional structure of the silica network prevents the achievement of a planar geometry of the $(-O)_3Si^+$ centre, thus supporting our choice. However, in actual dispersed silica a partial relaxation would be possible and could affect the reaction energies explicitly involving the silicon cation.

The calculations reported in this article have been performed with the GAUSSIAN 94 program package [14] and were done on an IBM RISC/6000 workstations. The B3LYP hybrid exchange-correlation functional was used for all the calculations. This functional is based on Becke's three parameter functional [15] including a Hartree–Fock exchange contribution with the nonlocal correction for the exchange potential proposed by Becke in 1988 [16], together with the nonlocal correction for the correlation energy provided by the the functional of Lee, Young, and Parr [17]. Molecular structures were optimized using the B3LYP expression above. It has already been demonstrated that this hybrid functional gives accurate optimized geometries for a wide range of molecules [18]. We used two basis sets of valence double-ζ and triple-ζ level augmented by polarization functions. A standard 6-31G* basis set was used for all geometry optimizations and harmonic frequencies calculations. Single point calculations with a 6-311G** basis set have been performed on the stationary points and employed in the computation of the thermodynamic stabilities. Full geometry optimizations were performed on the considered model molecules using the nonlocal functional described above. It has already been demonstrated that this density functional gives accurate optimized geometries of first and second row compounds, and, for large basis sets like those employed, accurate bond energies [19, 20].

Harmonic normal-mode frequencies have been calculated for the optimized structures, computing analytical energy second derivatives as programmed in GAUSSIAN 94. It has recently been shown for a reference group of 122 molecules that DFT methods, including the B3LYP potential, give harmonic frequencies in good agreement with experiment, with overall root mean square (rms) errors within 34 cm^{-1}

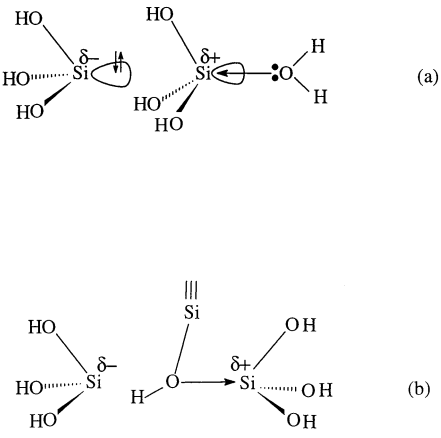

Scheme 1.

[21]. Following [21], we scaled the calculated frequencies by an optimum scaling factor, 0.9613, obtained by minimizing the residual errors between the experimental and calculated harmonic frequencies (using a BLYP functional and a 6-31G* basis set).

4. Results and discussion

4.1. The ionic configuration

The existence of an ionic state of the OBV defect in α quartz was first demonstrated by Snyder and Fowler [5] via Hartree–Fock calculations, and recently by Boero et al. [6] via Car–Parrinello calculations, and by Pacchioni et al. [7] via multireference configuration interaction (CI) (MRD CI) calculations. These authors modeled α quartz by means of small $(OH)_3Si–Si(OH)_3–OH_2$ clusters (the water molecule accounting for the effect of a lattice siloxane oxygen) and found a local minimum on the ground state surface corresponding to a "puckered" geometry with the Si atoms ~4 Å apart with a ≡Si–O═ distance of ~2 Å [see Scheme 1(a)].

This metastable configuration has been calculated ~2.7 eV higher than the ≡Si–Si≡ structure and can be described in terms of a doubly occupied dangling bond on one silicon atom and an empty sp^3 orbital on the other silicon that form a Lewis adduct with the water molecule [see Scheme 1(a)]. The situation, however, can be different when porous silica is considered. Porous silica is a reticulate polymer constituted by a network of random oriented and coiled chain, each chain being formed by $Si(O-)_4$ tetrahedra, occasionally terminated with OH groups [22, 23]. Whereas in α quartz the silicon atoms of the OBV defect remain in close proximity, thus favouring the formation of a ≡Si–Si≡ structure, the lower density of the dispersed silica introduces strain effects making the formation of silicon–silicon bonds more difficult. Moreover, at variance with α quartz, in dispersed silica there can be terminal silanol groups within the reticulate structure close to the OBV defect. The oxygen atom of these silanol groups can form a Lewis adduct with the silicon cation of the ionic configuration without requiring a puckering of the structure and preventing the formation of a Si–Si bond [see Scheme 1(b)]. Both effects stabilize the metastable ionic configuration with respect to the ≡Si–Si≡ structure, so that the former configuration is expected to play a more important role in dispersed silica than in α quartz.

4.2. The C_2H_4–OBV interaction

As discussed in the Introduction, the native oxygen bridge vacancy may exist in three different configurations corresponding to (1) a bonded silicon–silicon, (2) a diradical, and (3) a siloxane-stabilized ionic structure. Whereas the first state is expected to show a modest reactivity, the other two states are expected to be very reactive toward ethylene. We have performed a distinct theoretical study for each of these three configurations and their possible ethylene adducts.

4.2.1. Si–Si bonded configuration

The formation of a Si–Si bond can actually occur only if the energy gained in this process exceeds the energy required to strain the SiO_2 skeleton. In a previous article [9], we studied the energetics of the formation of a silicon–silicon bond, evaluating the strain effect of the silica network on this bond formation energy through the use of $(OH)_2Si^{\cdot}–O–^{\cdot}Si(OH)_2$ and

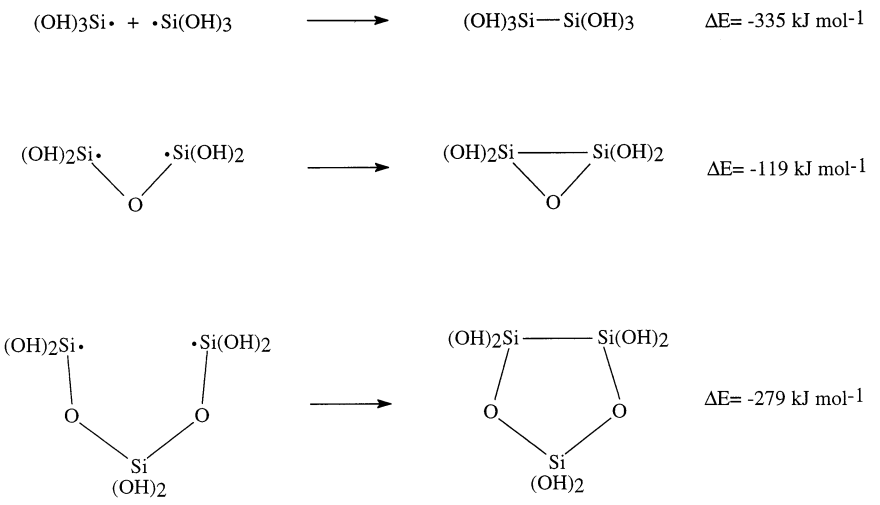

Scheme 2.

$(OH)_2Si^{\cdot}$–O–$Si(OH)_2$–O–$^{\cdot}Si(OH)_2$ diradical species in addition to two free $(OH)_3Si^{\cdot}$ radicals. This allowed us to simulate the recovery of the E″ centre formed by oxygen displacement in two- and three-membered ring structures of the silica network, leading to the results shown in Scheme 2.

Note that the Si–Si bond energy is 335 kJ mol^{-1} when a complete relaxation of the two $Si(OH)_3$ groups is allowed and, although substantially reduced by strain effects in cyclic species, remains fairly high in the three- and two-membered cycles (279 and 119 kJ mol^{-1}, respectively). The above results show that the C_2H_4 insertion between the silicon atoms is practically prevented except, possibly, for the most strained species. In that case, however, the reactivity will be determined by the diradical excited state and is discussed in the following section.

4.2.2. Diradical configuration

When the two silicon atoms are kept apart by the rigid silica structure, the E″ centre is constituted by two essentially noninteracting silicon radicals and is therefore expected to be strongly reactive. The reaction pathway is expected to involve the consecutive reactions of each of its constituting radicals. The first step of the ethylene insertion is, therefore, the addition of ethylene to one of the two radical centres to give a radical adduct:

$$(-O)_3Si^{\cdot} + CH_2{=}CH_2 \rightarrow (-O)_3Si{-}CH_2{-}CH_2^{\cdot}$$

We modeled this radical centre by a $(OH)_3Si^{\cdot}$ molecular species and considered the energetics of the formation of the radical adduct $(OH)_3Si{-}CH_2{-}CH_2^{\cdot}$, **9**. Table 1 reports the reaction energies computed for the addition of ethylene to $(OH)_3Si^{\cdot}$ and the possible evolution pathways of the initial radical adduct **9**. This radical species, with the unpaired electron on the β carbon, may undergo a hydrogen shift leading to an α-carbon radical $(OH)_3Si{-}CH^{\cdot}{-}CH_3$, **10**. Table 1 shows a high reaction energy for the addition of ethylene to the $(OH)_3Si^{\cdot}$ radical (125 kJ mol^{-1}), in agreement with the experimental evidence that the

Table 1
Reaction energies (kJ mol^{-1}) for ethylene reactions at one site of the E″ centre

Reaction	ΔE
$(OH)_3Si^{\cdot} + CH_2{=}CH_2 \rightarrow (OH)_3Si{-}CH_2{-}CH_2^{\cdot}$	−125
$(OH)_3Si{-}CH_2{-}CH_2^{\cdot} \rightarrow (OH)_3Si{-}CH^{\cdot}{-}CH_3$	−15
$(OH)_3Si{-}CH_2{-}CH_2^{\cdot} \rightarrow (OH)_3Si{-}CH{=}CH_2 + H^{\cdot}$	+164
$(OH)_3Si{-}CH_2{-}CH_2^{\cdot} \rightarrow (OH)_3Si{-}CH{=}CH^{\cdot} + H_2$	+189
$(OH)_3Si{-}CH^{\cdot}{-}CH_3 \rightarrow (OH)_3Si{-}CH{=}CH_2 + H^{\cdot}$	+182
$(OH)_3Si{-}CH^{\cdot}{-}CH_3 \rightarrow (OH)_3Si{-}C^{\cdot}{=}CH_2 + H_2$	unstable

Table 2
Reaction energies (kJ mol^{-1}) for ethylene reactions at the E″ centre

Reaction	ΔE
$2\ (OH)_3Si^{\cdot} + CH_2{=}CH_2 \rightarrow (OH)_3Si{-}CH_2{-}CH_2{-}Si(OH)_3$	−469
$2\ (OH)_3Si^{\cdot} + CH_2{=}CH_2 \rightarrow (OH)_3Si{-}CH(CH_3){-}Si(OH)_3$	−536
$2\ (OH)_3Si^{\cdot} + CH_2{=}CH_2 \rightarrow (OH)_3Si{-}CH{=}CH_2 + H{-}Si(OH)_3$	−391
$2\ (OH)_3Si^{\cdot} + CH_2{=}CH_2 \rightarrow (OH)_3Si{-}CH(=CH_2){-}Si(OH)_3 + H_2$	−361
$2\ (OH)_3Si^{\cdot} + CH_2{=}CH_2 \rightarrow (OH)_3Si{-}CH{=}CH{-}Si(OH)_3 + H_2$	−337

addition of a silyl radical to a carbon–carbon double bond is a remarkably facile process [24]. Indeed, the addition of silyl radicals to a carbon–carbon double bond is the key step in the hydrosilylation of alkenes [25,26]. The hydrogen shift leading to an α carbon radical is a slightly exothermic process, as expected, on the basis of the stability scale of organic radicals [27].

Both radicals can recombine with the adjacent second silicon radical of the E″ centre leading to a $-CH_2{-}CH_2-$ or $-CH(CH_3)-$ bridged species, $(OH)_3Si{-}CH_2{-}CH_2{-}Si(OH)_3$, **11**, and $(OH)_3Si{-}CH(CH_3){-}Si(OH)_3$, **12,** respectively. The relative abundance of the two species is determined by a subtle compromise between energetic and geometric factors. Indeed, although the α-carbon radical is 15 kJ mol^{-1} more stable than the β one, its formation involves a 1,2 hydrogen shift and is expected to have a substantial activation energy. Therefore, whenever allowed by the geometrical arrangement of the two silicon radicals of the E″ centre, the firstly formed α-carbon radical combines immediately with the adjacent silicon radical leading to the $-CH_2{-}CH_2-$ bridged species **11**, whereas for Si–Si distances too short to allow such a recombination, the lifetime of the α-carbon radical is high enough to allow the hydrogen shift and finally the formation of the $-CH(CH_3)-$ bridged species **12**.

Hydrogen abstraction, leading to a vinyl–silicon species $(OH)_3Si{-}CH{=}CH_2$, **13**, or a double hydrogen abstraction (as H_2 molecule), leading to a vinyl–silicon radical $(OH)_3Si{-}CH{=}CH^{\cdot}$, **14**, or $(OH)_3Si{-}C^{\cdot}{=}CH_2$, **15**, respectively, are thermodynamically unfavoured by about 150–200 kJ mol^{-1} and therefore quite unlikely.

The final results of the C_2H_4 interaction with the E″ centre can be obtained by considering the subsequent reaction of each of the evolution pathways of the first addition of the ethylene to one $(OH)_3Si^{\cdot}$ radical, considered above, with the the second silicon radical. All the considered reactions are reported in Table 2, together with the computed reaction energies. We see that the reactions leading to the $–CH_2–CH_2–$ or $–CH(CH_3)–$ bridged species **11** and **12** are both strongly exothermic (469 and 536 kJ mol^{-1}, respectively), thus confirming the assignment of [2]. Although most of the other possible reactions are also exothermic, they involve a single or double hydrogen abstraction and a sizeable energy barrier is therefore expected. The corresponding products (see Table 2) are thus quite unlikely, in agreement with the absence of any experimental evidence for them [2].

A geometrical optimization has been performed on all the molecules reported in Table 2 and some of the calculated geometries are illustrated in Fig. 4. The full set of harmonic frequecies have been calculated for **11** and **12** and those concerning the C–H stretching of the CH_2 or CH_3 groups are reported in Table 3. In Table 3 we also show the corresponding frequencies for the analogue organic molecules *n*-butane and *t*-butane. Note that whereas the frequencies calculated for the CH_3 group in *t*-butane agree with the experimental values observed for alkanes (2872 and 2962 $cm^{-1} \pm 10\ cm^{-1}$ [28]) within the expected error of 34 cm^{-1}, the frequencies calculated for the CH_2 group in *n*-butane deviate more appreciably from the experimental values observed for alkanes (2853 and 2926 $cm^{-1} \pm 10\ cm^{-1}$ [28]) thus making the assignments more questionable from a purely theoretical point of view. A correct attribution of the the experimentally observed C–H stretching bands on the basis of the frequencies calculated for **11** and **12** is therefore not straightforward, since the accuracy of our calculations

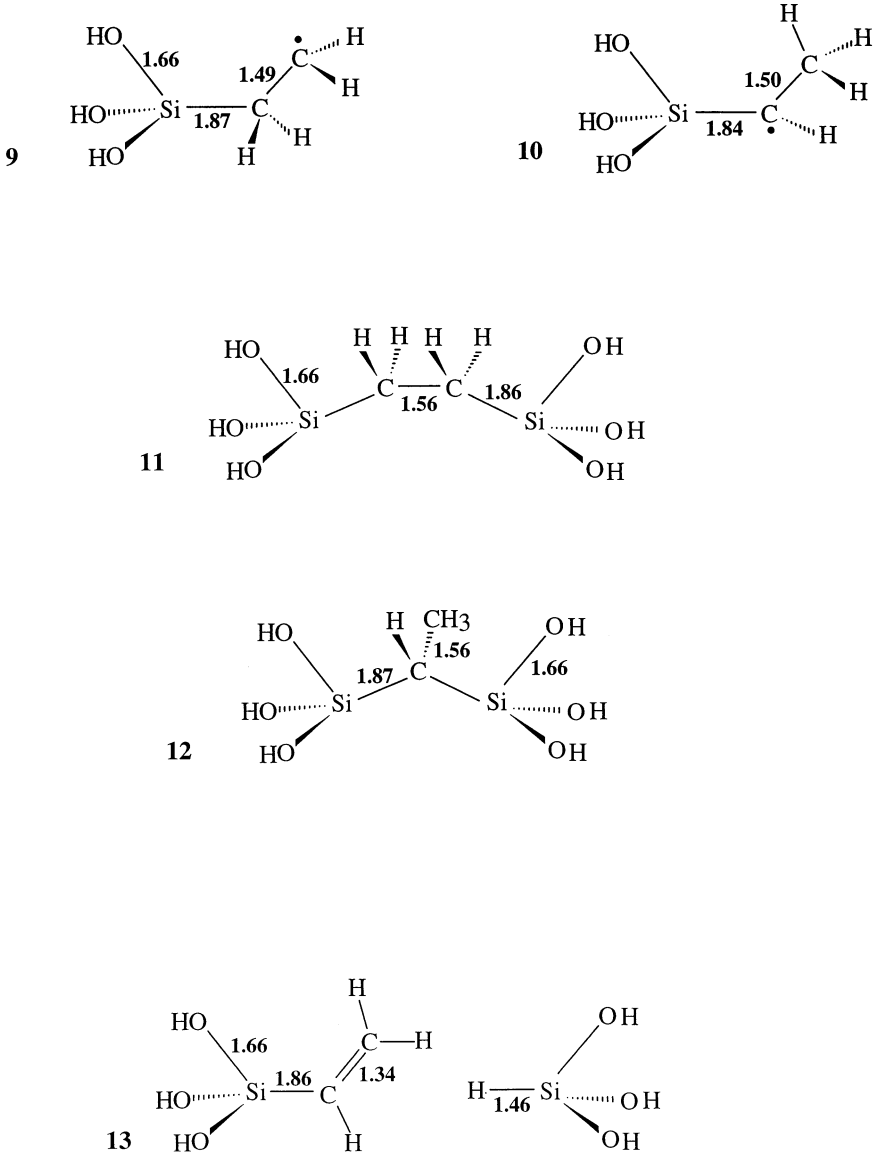

Fig. 4. Optimized geometries of some considered models for ethylene adducts on the E″ centre.

is of the order of the difference between symmetric and asymmetric stretching of CH_2 and CH_3 groups (the considered bands). Some useful conclusions can, however, be drawn from our results by taking into account a comparison between the calculated and experimental C–H stretching frequencies of *n*-butane and *t*-butane and further considerations concerning the $–CH_2–CH_2–$ bridged cyclic species **16** and **17**.

The C–H stretching frequencies have been calculated at 2908 and 2971 cm^{-1} for the CH_2 group in **11** and 2914 and 2976 cm^{-1} for the CH_3 group in **12** and are very close to the corresponding frequencies for the organic analogues (*n*-butane and *t*-butane) at 2913 and 2959 cm^{-1} and 2916 and 2984 cm^{-1}, respectively (see Table 3).

The use of molecules **11** and **12** as models of the

Table 3
Harmonic scaled frequencies (cm^{-1}) and intensities (kM cm^{-1}) in parentheses for the symmetric and antisymmetric C–H stretching of CH_2 and CH_3 groups in $(OH)_3Si–CH_2–CH_2–Si(OH)_3$, **11**; *cyclo*—$(OH)_2Si–CH_2–CH_2–Si(OH)_2$, **16**; *cyclo*—$(OH)_2Si–CH_2–CH_2–Si(OH)_2$, **17**; $(OH)_3Si–CH(CH_3)–Si(OH)_3$, **12**; *n*-butane and *t*-butane. In the last two rows the experimental values observed for the as-implanted and annealed samples, respectively, are reported

Mode assignment	Symmetric	Antisymmetric
11	2908	2971
16	2943	3009
17	2915	2982
12	2914	2976
n-butane	2913	2959
t-butane	2916	2984
as-implanted (CH_2)	2860	2936
as-implanted (CH_3)	2880	2970

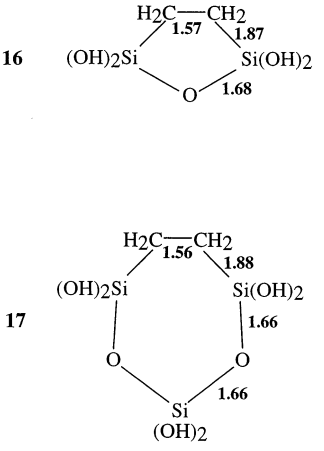

Fig. 5. Optimized geometries of the cyclic models for $–CH_2–CH_2–$ bridging of the E″ centre.

$–CH_2–CH_2–$ and $-CH(CH_3)-$ bridges in the solid state allows a complete relaxation of the two $Si(OH)_3$ groups and completely describes unstrained bridges. However, it is known that the C–H stretching frequencies of the CH_2 group are shifted to higher frequencies in cyclic hydrocarbons because of the ring strain (more than 20 cm^{-1} for cyclobutane with respect to *n*-butane) [28]. Therefore, we expect a shift to higher frequencies because of the strain imposed on the bridge by the rigid structure of the silica network. This was already pointed out by Cerofolini et al. [2], who assigned the shift toward higher frequencies of the C–H stretching observed for the as-implanted sample (~10 cm^{-1} with respect to the frequencies observed in alkanes) to strain effects and the decrease to values more typical of alkane upon annealing to a release of the strain.

Indeed, it is known that the network of porous silica is constituted mainly by three-, four-, five- and six-membered rings (i.e. cyclic structures made up by three, four, five, or six silicon atoms connected by oxygen atoms) fused together to form the three-dimensional network [22, 23]. Therefore, when an E″ centre is formed by an oxygen displacement, the two silicon radicals are part of an open three-, four-, five-, or six-membered ring, respectively. The formation of the $–CH_2–CH_2–$ bridge between the two silicon atoms will therefore lead to a cyclic silicon bridged species.

These strained species, actually fused within the silica three-dimensional network, have been modeled by discrete cyclic molecules. We considered only the most strained species with two and three silicon atoms, **16** and **17** (see Fig. 5), assuming that the C–H stretching in four or higher membered rings is essentially the same as that calculated for the acyclic molecule **4**. A geometry optimization has been performed on these two molecules, and the corresponding vibrational spectra calculated (see Table 3). We see that the the C–H stretching frequencies of CH_2 calculated for the three-membered molecule **17** are shifted 7–11 cm^{-1} with respect to the unstrained molecule **11**. A substantially higher frequency has been calculated for the two-membered cyclic molecule **16** (35–38 cm^{-1}) but it is known that two-membered rings are highly improbable in disperse silica [23]. These results confirm the assignments of [2] showing that strain effects of the order of those expected to operate in the silica framework can be responsible for the shift of C–H stretching of CH_2 with respect to alkanes observed in the as-implanted sample.

4.2.3. Ionic configuration

In this case, the OBV defect is constituted by two silicon ions ~4 Å apart, with the silicocation stabilized by a coordinate siloxane or silanol oxygen:

Table 4
Reaction energies (kJ mol^{-1}) for ethylene reactions at one silicocation of the ionic configuration

Reaction	ΔE
$(OH)_3Si^+ + CH_2{=}CH_2 \rightarrow [(OH)_3Si(CH_2{=}CH_2)]^+$	−384
$[(OH)_3Si(CH_2{=}CH_2)]^+ \rightarrow (OH)_3Si{-}CH_2{-}CH_2^+$	+4
$(OH)_3Si{-}CH_2{-}CH_2^+ \rightarrow (OH)_3Si{-}CH^+{-}CH_3$	+81

$(-O)_3Si^+ \leftarrow :O\langle\ ^-Si(O-)_3$. This configuration is expected to be less reactive than the diradical toward ethylene and to involve an acid-base pathway. Because of the nucleophilic nature of the ethylene molecule, the first step of its interaction with the ionic pair is expected to be the cordination to the silicon cation centre:

$$(-O)_3Si^+ + C_2H_4 \rightarrow (-O)_3Si^+(CH_2{=}CH_2)$$

with a possible displacement of the coordinated siloxanic oxygen. As long as the geometry of the OBV defect in this ionic configuration remains unperturbed, such an ionic ethylene adduct is expected to be stable. Upon annealing, the E″ centre may relax to a different geometry allowing the formation of a $-CH_2-CH_2-$ species, probably via a silicon carbocation intermediate $(-O)_3Si{-}CH_2{-}CH_2^+$.

We have modeled the ionic configuration with two $(OH)_3Si^+$ and $(OH)_3Si^-$ ions and computed energies for the coordination of ethylene to the silicocation and its subsequent evolution to a carbocation and a bridged species (see Table 4). First of all, we see from Table 4 that the coordination of ethylene to a $(OH)_3Si^+$ cation is a thermodynamically very favourable process by 384 kJ mol^{-1}. In principle, ethylene can displace the siloxane or silanol oxygen stabilizing the ionic pair only if its coordination energy is higher than that of these $\equiv Si^+ \leftarrow :O\langle$ Lewis adducts. The coordination of a siloxane or silanol group to a silicocation has been modeled by that of a water molecule to a $(OH)_3Si^+$ ion and led to a coordination energy of 479 kJ mol^{-1}. Although this result would not support the displacement of the siloxane or silanol oxigen by ethylene, we should take into account that in the real three-dimensional structure of silica the coordination energy of siloxane or silanol groups is strongly affected by strain energy and can be considerably reduced with respect to the value for a completely free water molecule. The calculations performed on the Si–Si bond formation energy show that this strain effect can easily give contributions up to 200 kJ mol^{-1}, so that ethylene could effectively bind to the silicon cation of strained ionic configurations.

On the basis of the analogy with the carbocation chemistry [27], we expect that the π-coordinated $[(OH)_3Si(CH_2{=}CH_2)]^+$ species, **18**, may evolve to a silicon carbocation $[(OH)_3Si{-}CH_2{-}CH_2^+]$, **19**, and then undergo a hydryde shift to $[(OH)_3Si{-}CH^+{-}CH_3]$, **20**. Table 4 shows that the β-carbon carbocation **19** is slightly higher than the π-coordinated species **18** (4 kJ mol^{-1}) and is therefore a viable intermediate in the formation of a $-CH_2-CH_2-$ bridge. The positive charge transfer from silicon to β carbon is also expected to be facilitated by the increase of electrostatic pairing energy $-CH_2^+{}^-Si(O-)_3$. It is worth noting that the Si–Si separation in the ionic configuration $[(-O)_3Si^+ \leftarrow :O\langle\ ^-Si(O-)_3]$ is ~4 Å and therefore perfectly suited to allow the formation of a second Si–C bond between the β carbon of silicon carbocation and the silicon anion (compare with the Si–Si distance of 4.2 Å in **11**). The instability of the α-carbon carbocation **20** (81 kJ mol^{-1} higher than **19**) and the unsuitable geometry of the ionic configuration would prevent the formation of a $-CH(CH_3)-$ bridge. These results are in good agreement with the experimental IR evidence showing the simultaneous disappearence of the adsorbed-ethylene signal and the increase of the CH_2 signal upon annealing.

A quantitative description of the metastable ionic configuration requires flexible cluster models and an extensive inclusion of the correlation effects that is hardly feasible within DFT calculations on simple molecular models. Therefore, we did not perform an accurate calculation of the reaction energy for the ethylene addition to the ionic configuration:

$$(-O)_3Si^+ \leftarrow :O\langle\ ^-Si(O-)_3 + CH_2{=}CH_2 \rightarrow$$

$$(OH)_3Si{-}CH_2{-}CH_2{-}Si(OH)_3 + :O\langle \qquad (2)$$

However, calculations performed on α quartz [5] pose the ionic configuration ~260 kJ mol^{-1} higher in energy than the Si–Si bonded ground state that, in our energy scale based on Scheme 2, corresponds to ~60 kJ mol^{-1} below the diradical state. Therefore, a rough evaluation of the reaction energy for reaction (2) can be obtained by subtracting 60 kJ mol^{-1} from the reaction energy relative to the diradical state reported in Table 2. A value on the order of 400 kJ mol^{-1} is obtained, showing that the addition of ethylene to the ionic configuration leading to a $-CH_2$–CH_2- bridge is a thermodynamically favoured process. However, the higher energy of **19** with respect to **18** would suggest that this is a thermally activated process, thus explaining its occurrence only upon annealing.

A geometrical optimization has been performed on molecules **18**–**20** and their geometries are illustrated in Fig. 6. The C═C stretching in **18** has been calculated at 1583 cm^{-1}, showing a significant shift to lower frequencies compared to free ethylene, and strongly supports the assignments of the observed peak at 1581 cm^{-1} proposed in [2]. The satellite peak at 1640 cm^{-1} falls very close to the C═C stretching for free etylene and is probably due to weakly adsorbed or trapped ethylene.

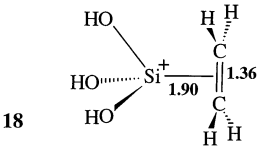

18

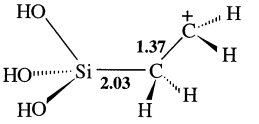

19

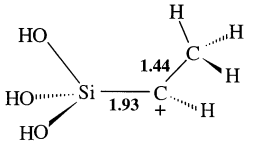

20

Fig. 6. Optimized geometries of the considered models for ethylene adducts on the ionic configuration.

4.3 The C_2H_4–SLV interaction

4.3.1. Recovery to a PSL form

Because the SLV centre associated with the oxygen-bridge vacancy is made up of four close ≡Si–O˙ radicals, a simple recovery mechanism is available with the formation of a bond between one or two pairs of oxygen atoms leading, respectively, to a partial or total PSV. Analogous to that observed for the recovery of the E″ centre, the formation of an O–O bond can actually occur only if the energy gained in this process exceeds the energy required to strain the SiO_2 skeleton. However, in this case the higher degree of freedom of the ≡Si–O˙ radicals allow us to more easily satisfy these strain requirements. Therefore, we studied the energetics of the formation of an oxygen–oxygen bond simulating the system with two free $(OH)_3Si–O˙$ radicals

$$2(OH)_3Si–O˙ \rightarrow (OH)_3Si–O–O–Si(OH)_3 \quad (3)$$

We calculated an O–O bond energy of 85 kJ mol^{-1} (with an O–O distance of 1.437 Å) that is expected to be further reduced whenever strain effects are operating. This result suggests that, even when a complete relaxation of the SLV to PSV is allowed, only a limited activation energy is required to cleave this peroxidic bridge.

4.3.2. Radical configuration

When the SLV is seen as constituted by four ≡Si–O˙ radicals, it is expected to be strongly reactive toward ethylene. We ignored the possible interaction between the four $(-O)_3Si–O˙$ radicals, assuming a reaction pathway involving the consecutive reactions of ethylene with only two out of the four possibly available radicals. Therefore, we modeled the SLV centre with two $(OH)_3Si–O˙$ molecular species, using essentially the same approach followed for the E″ centre. The first step of the ethylene insertion is still

Table 5
Reaction energies (kJ mol^{-1}) for ethylene reactions at one site of the SLV centre

Reaction	ΔE
$(OH)_3SiO^{\cdot} + CH_2{=}CH_2 \rightarrow (OH)_3SiO{-}CH_2{-}CH_2^{\cdot}$	−100
$(OH)_3SiO{-}CH_2CH_2^{\cdot} \rightarrow (OH)_3SiO{-}CH^{\cdot}{-}CH_3$	−50
$(OH)_3SiO{-}CH_2{-}CH_2^{\cdot} \rightarrow (OH)_3SiO{-}CH{=}CH_2 + H^{\cdot}$	+151
$(OH)_3SiO{-}CH_2{-}CH_2^{\cdot} \rightarrow (OH)_3SiO{-}CH{=}CH^{\cdot} + H_2$	+202
$(OH)_3SiO{-}CH^{\cdot}{-}CH_3 \rightarrow (OH)_3Si{-}O{-}CH{=}CH_2 + H^{\cdot}$	+203
$(OH)_3SiO{-}CH^{\cdot}{-}CH_3 \rightarrow (OH)_3SiO{-}C^{\cdot}{=}CH_2 + H_2$	+198
$(OH)_3SiO{-}CH^{\cdot}{-}CH_3 \rightarrow (OH)_3Si^{\cdot} + CH_3CHO$	+136

expected to be the addition of ethylene to one of the two radical centres to give a radical adduct:

$$(-O)_3SiO^{\cdot} + CH_2{=}CH_2 \rightarrow (-O)_3SiO^{-}CH_2{-}CH_2^{\cdot}$$

We modeled this radical centre by a $(OH)_3Si{-}O^{\cdot}$ molecular species and considered the energetics of the formation of the radical adduct $(OH)_3SiO{-}CH_2{-}CH_2^{\cdot}$, **21**. Table 5 reports the reaction energies computed for the addition of ethylene to $(OH)_3SiO^{\cdot}$ and the possible evolution pathways of the initial radical adduct **21**. This radical species, with the unpaired electron on the β carbon, may undergo a hydrogen shift leading to an α-carbon radical $(OH)_3SiO{-}CH^{\cdot}{-}CH_3$, **22**. Table 5 shows that the addition of ethylene to the $(OH)_3SiO^{\cdot}$ leading to a β-carbon radical is an exothermic process (100 kJ mol^{-1}) and that, on the basis of the favourable energy difference (50 kJ mol^{-1}), the latter radical is expected to evolve spontaneously to the α-carbon isomer.

Both radicals can recombine with the adjacent second oxygen radical leading to a $-CH_2{-}CH_2-$ or $-CH(CH_3)-$ bridged species:

$(OH)_3SiO{-}CH_2{-}CH_2{-}OSi(OH)_3$, **23**

$(OH)_3SiO{-}CH(CH_3){-}OSi(OH)_3$, **24**

In principle, these radicals might also undergo hydrogen abstraction leading to a vinyl-silicon species $(OH)_3SiO{-}CH{=}CH_2$, **25**, or a double hydrogen abstraction (as H_2 molecule) leading to a vinyl-silicon radical $(OH)_3SiO{-}CH{=}CH^{\cdot}$, **26**, or $(OH)_3SiO{-}C^{\cdot}{=}CH_2$, **27**, respectively. However, all these reactions are thermodynamically unfavoured by about 150–200 kJ mol^{-1} and therefore quite unlikely.

We have then considered the final results of the C_2H_4 interaction with the SLV centre by examining the consecutive reaction of each of the evolution pathways of the first addition of the ethylene to one $(OH)_3SiO^{\cdot}$ radical, considered above, with the the second oxygen radical. All the considered reactions are reported in Table 6, together with the computed reaction energies. We see that the reactions leading to the $-CH_2{-}CH_2-$ or $-CH(CH_3)-$ bridged species **23** and **24** are both strongly exothermic (457 and 461 kJ mol^{-1}, respectively). However, in this case, there is an alternative, more favourable pathway, unavailable for the E″ centre, which is the hydrogen abstraction by the second ≡Si–O$^{\cdot}$ radical, leading to a silanol unit and the silyl vinyl ether **25**:

$$\begin{matrix}(OH)_3SiO{-}CH_2{-}CH_2^{\cdot}\\(OH)_3SiO{-}CH^{\cdot}{-}CH_3\end{matrix} + {}^{\cdot}OSi(OH)_3 \rightarrow$$

$$(OH)_3Si{-}O{-}CH_2{=}CH_2 + HOSi(OH)_3$$

Table 6
Reaction energies (kJ mol^{-1}) for ethylene reactions at the SLV centre

Reaction	ΔE
$2\ (OH)_3SiO^{\cdot} + CH_2{=}CH_2 \rightarrow (OH)_3SiO{-}CH_2{-}CH_2{-}OSi(OH)_3$	−457
$2\ (OH)_3SiO^{\cdot} + CH_2{=}CH_2 \rightarrow (OH)_3SiO{-}CH(CH_3){-}OSi(OH)_3$	−461
$2\ (OH)_3SiO^{\cdot} + CH_2{=}CH_2 \rightarrow (OH)_3SiO{-}CH{=}CH_2 + HOSi(OH)_3$	−466
$2\ (OH)_3SiO^{\cdot} + CH_2{=}CH_2 \rightarrow (OH)_3Si{-}O{-}Si(OH)_3 + CH_3CHO$	−535
$2\ (OH)_3SiO^{\cdot} + CH_2{=}CH_2 \rightarrow (OH)_3SiO{-}C(=CH_2){-}OSi(OH)_3 + H_2$	−342
$2\ (OH)_3SiO^{\cdot} + CH_2{=}CH_2 \rightarrow (OH)_3SiO{-}CH{=}CH{-}OSi(OH)_3 + H_2$	−325
$2\ (OH)_3SiO^{\cdot} + CH_2{=}CH_2 \rightarrow (OH)_3Si{-}Si(OH)_3 + CH_3COOH$	−251
$2\ (OH)_3SiO^{\cdot} + CH_2{=}CH_2 \rightarrow 2\ (OH)_3SiOH + CH{\equiv}CH$	−301

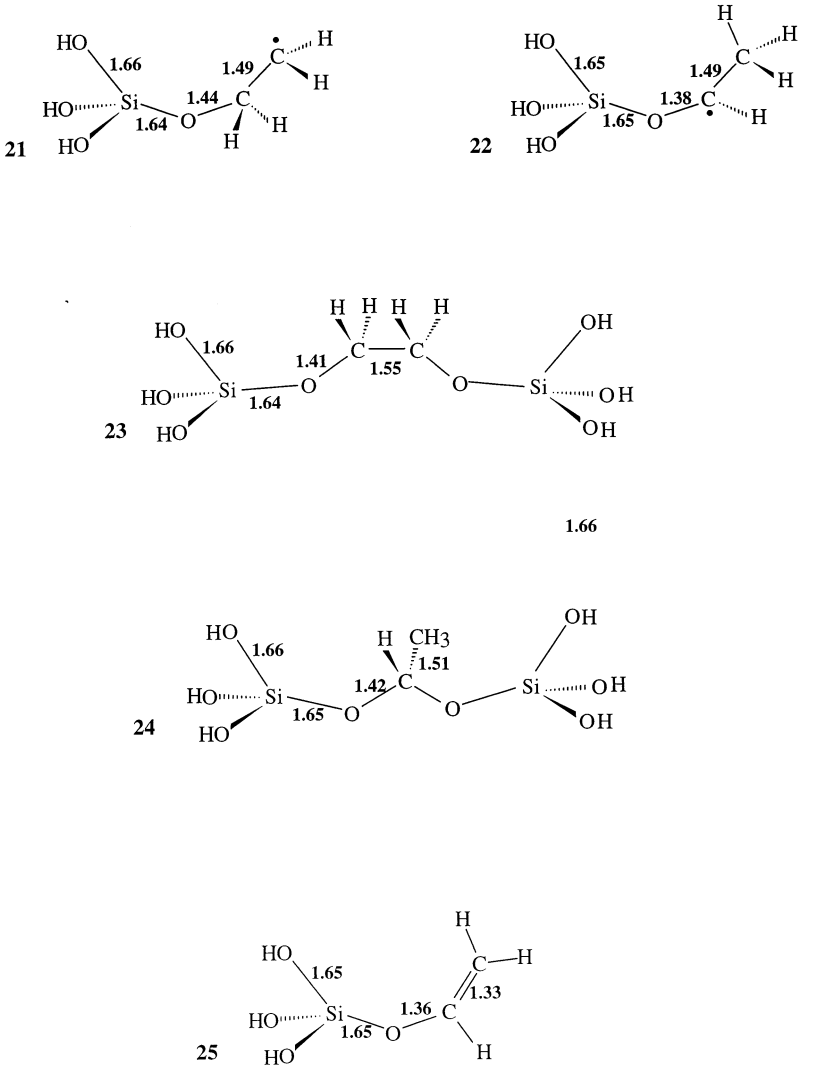

Fig. 7. Optimized geometries of the considered models for ethylene adducts on the SLV defect.

Such a process has been calculated for 9 and 5 kJ mol^{-1}, respectively, more exothermic than the formation of $–CH_2–CH_2–$ or $–CH(CH_3)–$ bridges. Moreover, while the formation of $–CH_2–CH_2–$ and $–CH(CH_3)–$ bridges requires a suitable geometrical arrangement of the two $\equiv Si–O^{\cdot}$ radicals and might require a significant strain energy, the vinyl silyl ether may form without any of these requirements so that it is expected to be the main product. Note that such a species corresponds to the hypothesized centre **8** of [2]. However, this vinyl silyl ether is expected to be unstable in the presence of an adjacent silanol group and to evolve to acetic aldehyde and a siloxane bond:

$$(OH)_3Si–O–CH{=}CH_2HO–Si(OH)_3 \rightarrow (OH)_3Si–O–Si(OH)_3 + CH_3CHO \quad (4)$$

probably through an attack of the silanol oxygen to the electrophilic silicon atom of the vinyl silyl ether.

Table 6 shows that this reaction is exothermic by 69 kJ mol^{-1} and leads to the most stable products among the ones that have been hypothesized for the etylene addition to the SLV defect (by 535 kJ mol^{-1}). This is in agreement with the experimental evidence, interpreted in terms of formation of acetic aldehyde after annealing. A geometry optimization has been performed on all the molecules reported in Tables 5 and 6 and some of the calculated geometries are illustrated in Fig. 7.

All the other possible reactions reported in Table 6 are much less exothermic and involve a single or double hydrogen abstraction with an expected sizeable energy barrier. Therefore, the corresponding products are not expected to form, in agreement with the absence of any experimental evidence for them [2].

5. Conclusions

In this article quantum chemical modeling is applied to interpret the results of an experimental infrared characterization of the addition of C_2H_4 to the SiO_2 skeleton at the diradical silicon defect produced by argon bombardment. Accurate DFT calculations have been performed on suitable models of the silica OBV and SLV defects and their C_2H_4 adducts. The results are consistent with a previous interpretation of the IR data, according to which the addition of C_2H_4 to the oxygen-bridge vacancy takes place either via a radical pathway leading to $-CH_2-CH_2-$ or $-CH(CH_3)-$ bridges between the silicon centres or via an acid-base mechanism initially leading to an ionic pair with the ethylene moiety coordinated to the cationic unit.

On the other hand, the addition of C_2H_4 to the silicon-link vacancy takes place place only via a radical pathway leading to a silicon vinyl ether species that then evolves to an acetic aldehyde and a siloxane bridge.

The calculations on the molecular models show that the proposed derivatives are stable species and yield C═C and C–H stretching frequencies which confirmed the assignments of the experimentally observed values proposed in [2].

Acknowledgements

This work has been carried out within the CNR strategic project for Computational Modeling of Complex Molecular Systems. We thank the CINECA for providing a computer grant.

References

[1] G.F. Cerofolini, L. Meda, C. Spaggiari, G. Conti, G.M. Garbasso, J. Chem. Soc., Faraday Trans. 92 (1996) 2453.
[2] G.F. Cerofolini, G. Conti, G.M. Garbasso, C. Spaggiari, L. Meda, Nucl. Instrum Methods 92 (1996) 49.
[3] G.F. Cerofolini, N. Re, in Fundamental Aspects of Ultrathin Dielectrics on Si-Based Devices: Towards an Atomic-Scale Understanding, E. Garfunkel, E. Gusevand, A. Vul (Eds.), Kluwer, Dordrecht, 1997, pp. 117.
[4] J.K. Rudra, W.B. Fowler, Phys. Rev. B 35 (1987) 8223.
[5] K.C. Snyder, W.B. Fowler, Phys. Rev. B 48 (1993) 13238.
[6] M. Boero, H. Pasquarello, J. Sarnthein, R. Car, Phys. Rev. Lett. 78 (1997) 887.
[7] G. Pacchioni, G. Ieranò, Phys. Rev. Lett. 79 (1997) 753.
[8] G.F. Cerofolini, A. Anselmino, L. Meda, G. Ranghino, Mater. Res. Soc. Symp. Pros. 431 (1996) 303.
[9] N. Re, A. Sgamellotti, G.F. Cerofolini, J. Phys. Chem. B 101 (1997) 9695.
[10] J. Sauer, Chem. Rev. 89 (1989) 199.
[11] J. Sauer, P. Ugliengo, E. Garrone, V.R. Saunders, Chem. Rev. 89 (1989) 199.
[12] E. Garrone, P. Ugliengo, in Structure and Reactivity of Surfaces, A. Zecchina, G. Costa, C. Morterra (Eds.), Elsevier, Amsterdam, 1989.
[13] P. Ugliengo, V.R. Saunders, E. Garrone, J. Phys. Chem. 93 (1989) 5210.
[14] M.J. Frisch, G.W. Trucks, H.M. Schlegel, P.M.W. Gill, B.G. Johnson, M.W. Wong, J.B. Foresman, M.A. Robb, M. Head-Gordon, E.S. Replogle, R. Gomperts, J.L. Andres, K. Raghavachari, J.S. Binkley, C. Gonzales, R.L. Martin, D.J. Fox, D.J. Defrees, J. Baker, J.J.P. Stewart, J.A. Pople, GAUSSIAN 94 (Revision A.1), Gaussian Inc., Pittsburgh, PA, 1994.
[15] A.D. Becke, J. Chem. Phys. 98 (1993) 5648.
[16] A.D. Becke, Phys. Rev. A 38 (1988) 2398.
[17] C. Lee, W. Young, R.G. Parr, Phys. Rev. B 37 (1988) 785.
[18] C.W. Bauschlicher Jr., Chem. Phys. Lett. 246 (1995) 40.
[19] T. Ziegler, Chem. Rev. 91 (1991) 651.
[20] T. Ziegler, Can. J. Chem. 73 (1995) 743.
[21] M.W. Wong, Chem. Phys. Lett. 256 (1996) 391.
[22] K.D. Keefer, in Silicon-Based Polymer Science: A Comprehensive Resource, J.M. Zeigler, F.W. Gordon Fearon (Eds.),

Adv. Chem. Ser. No. 224, American Chemical Society, Washington DC, 1990.
[23] C.J. Brinker, G.W. Scherer, Sol-Gel Science, Academic, London, 1990.
[24] C. Chatgilialoglu, Chem. Rev. 95 (1995) 1229.
[25] R.A. Jackson, Adv. Free Radical Chemistry 3 (1969) 231.
[26] H. Sakurai, in Free Radicals, J.K. Kochi (Ed.), Wiley, New York, 1973, Vol. II, p. 741.
[27] J. March, Advanced Organic Chemistry, McGraw-Hill, New York, 1991.
[28] L.J. Bellamy, The Infrared Spectra of Infrared Molecules, Chapman and Hall, London, 1975, Vol. 1.